Biochemistry

pubs.acs.org/biochemistry Article

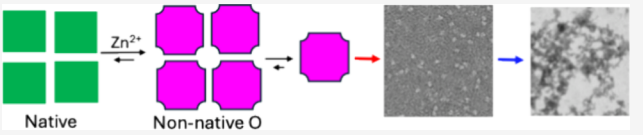
# $Zn^{2+}$-Induced Dissociation of Transthyretin Tetramers Generates Toxic, Seeding-Active Misfolded Oligomers

Robert Irving, Anvesh Dasari, Sy Duke, Sungsool Wi, Robert M. Hughes, Anne M. Spuches, and Kwang Hun Lim*

Cite This: *Biochemistry* 2026, 65, 3017−3025 Read Online

ACCESS | Metrics & More | Article Recommendations | Supporting Information

**ABSTRACT:** The aggregation of transthyretin (TTR) is a hallmark of ATTR amyloidosis. Accumulating evidence suggests that metal ions, particularly $Zn^{2+}$, promote TTR aggregation; however, the molecular mechanism underlying $Zn^{2+}$-induced misfolding remains poorly understood. Here, we present a comprehensive biophysical characterization of $Zn^{2+}$-induced misfolding of wild-type transthyretin (TTRwt) under physiologically relevant conditions. Two-dimensional $^{1}H/^{15}N$ HSQC NMR analyses reveal that $Zn^{2+}$ binding induces millisecond-time scale conformational exchange that destabilizes the native tetramer. These structural and dynamic perturbations promote the formation of small, toxic oligomeric species capable of self-propagation through the seeding of native TTR. Comparative structural analyses using solid-state NMR also show that $Zn^{2+}$-induced oligomers adopt broadly native-like secondary structures, but exhibit distinct non-native molecular conformations. The early stages of misfolding were further investigated using $^{19}F$ NMR of TTRwt containing fluorinated tryptophan residues. Notably, $^{19}F$ NMR not only reports on $Zn^{2+}$ binding but also enables direct detection of a transient monomeric intermediate generated upon tetramer dissociation, a key species in the amyloidogenic cascade. Together, these findings define the structural and dynamic basis of $Zn^{2+}$-mediated TTR misfolding and establish combined solution and solid-state NMR approaches as powerful tools for probing metal-induced misfolding landscapes in TTR and related amyloidogenic proteins.




## INTRODUCTION

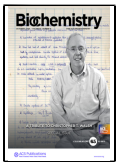
Transthyretin (TTR) is a 55 kDa homo-tetramer transporter protein that participates in transporting retinol and thyroxine to the liver.[1,2] Deposition of TTR aggregates affects various organs, particularly the heart and peripheral nerves, causing cardiomyopathy and polyneuropathy (ATTR amyloidosis).[3,4] Misfolding and aggregation of wild-type TTR (TTRwt) is associated with amyloid cardiomyopathy (ATTRwt-CM) that can cause life-threatening heart failure and arrhythmias, affecting as much as 25% of the population over age 80.[5−8] Over 120 pathogenic single-point mutations observed across the protein accelerate this misfolding and aggregation process, leading to an earlier onset of the diseases (ATTRv).[4]

Previous studies have shown that under partially denaturing conditions, tetrameric native TTR undergoes dissociation into aggregation-prone monomers, which then self-assemble into oligomers and larger aggregates, including fibrils.[9−11] Although pathogenic mutations destabilize native TTR and promote misfolding, the tetrameric native TTR, particularly TTRwt, remains highly stable at cellular TTR concentrations of 0.2−0.4 mg/mL under physiological pH. Recent studies have suggested that cellular environments play critical roles in misfolding and aggregation, with metal ions in these environments acting as potential aggregation promoters in vivo due to their strong influence on protein aggregation properties.[12−16] Indeed, metal ions such as $Zn^{2+}$ and $Ca^{2+}$ have been shown to accelerate TTR aggregation,[17] and elevated levels of these metal ions have been observed in ex vivo TTR aggregates,[18,19] indicating that they may trigger TTR aggregation in vivo.

Despite increasing evidence that metal ions promote TTR aggregation, the molecular mechanism by which metal binding perturbs the native tetramer under physiological conditions remains unresolved. In particular, the dynamic intermediates that connect metal binding to tetramer destabilization and oligomer formation have not been directly observed. Resolving these early structural events is essential for understanding how physiological metal ions initiate the amyloidogenic cascade. $^{19}F$ NMR has been utilized to detect intermediate states formed during aggregation process.[20−26] In particular, monomeric and dimeric intermediates dissociated from native tetramers were successfully identified by using trifluoroacetyl $^{19}F$ NMR probe attached to the site near to the interfacial region.[20,21]

Here, we report the molecular basis of $Zn^{2+}$-induced TTR misfolding and toxic oligomer formation with a combined use of TEM and NMR spectroscopy. In addition to conventional

Received: May 21, 2026
Revised: August 27, 2026
Accepted: September 3, 2026
Published: September 17, 2026



Downloaded from pubs.acs.org/bichaw/article-pdf/65/19/3017/6854085/acs.biochem.6c00448.pdf by FLORIDA STATE UNIV user on 02 November 2026


© 2026 American Chemical Society

https://doi.org/10.1021/acs.biochem.6c00448
*Biochemistry* 2026, 65, 3017−3025

$^{1}H/^{15}N$ HSQC and $^{13}C-^{13}C$ solid-state NMR spectroscopy, the early stages of misfolding were investigated using $^{19}F$ NMR of TTRwt containing fluorinated tryptophan residues (F6-Trp-TTRwt). Notably, $^{19}F$ NMR not only reports on $Zn^{2+}$ binding but also enables direct detection of a transient monomeric intermediate generated upon tetramer dissociation, a key species in the amyloidogenic cascade. These combined biophysical analyses provide mechanistic insights into TTR misfolding triggered by $Zn^{2+}$ binding under physiological pH conditions.

## METHODS AND MATERIALS

### Preparation of Recombinant TTR

TTR proteins were expressed in a bacterial expression system using the pMMHa plasmid, which does not encode a His-tag, as previously described.[9,27] Escherichia coli cells (BL21(DE3)) were cultured in Miller's LB Broth under constant agitation (250 rpm, 27°C). The bacterial cells were grown until an optical density at 600 nm ($OD_{600}$) reached 0.6−0.8 before induction with 1 mM isopropyl ß-D-1-thiogalactopyranoside (IPTG) for overexpression. The cells were incubated for an additional 12−14 h at 25°C before harvesting via centrifugation (8,000 rpm, 4°C). For NMR experiments, isotopically labeled TTR proteins were cultured instead in M9 medium containing $^{15}N$-enriched $NH_4Cl$ and $^{13}C$-enriched D-glucose following the same procedure as unlabeled TTR expression. The bacterial cells were resuspended using Tris lysis buffer [10 mM Tris, 150 mM NaCl at pH 8.0] before sonication to disrupt the pellet. Centrifugation at 13,000 rpm was utilized to collect the soluble fraction of the resuspended solution, with high-molecular weight impurities being removed via ammonium sulfate precipitation (50% wt/vol). The supernatant collected via centrifugation was dialyzed against Tris buffer [25 mM Tris, 1 mM PMSF, and 1 mM EDTA pH 8.0] overnight at 4°C. The protein was purified further using anion exchange chromatography [Cytivia HiTrap 5 mL Q HP; 20 mM Tris and 1 mM EDTA (pH 8.0)] and size exclusion chromatography [Cytiva HiLoad 16/600 Superdex 200 pg; 10 mM sodium phosphate buffer (pH 7.4)]. The proteins were then buffer exchanged into bis-tris buffer for experiments using a desalting column [Cytiva HiTrap 5 mL Desalting; 50 mM bis-tris and 150 mM NaCl, (pH 7.0)]. Protein absorbance was measured at 280 nm (ThermoScientific Evolution 201 UV−vis Spectrophotometer) with the concentration calculated using an extinction coefficient of 77,600 $M^{-1}$ $cm^{-1}$ and molecular weight of 55,044 g/mol.

For incorporation of 6-fluorotryptophan (6F-Trp) into TTR, *E. coli* cells were grown in M9 minimal medium to an optical density at 600 nm ($OD_{600}$) of approximately 0.6. A mixture of aromatic amino acids (phenylalanine, tyrosine, and 6-fluorotryptophan; 50 mg/L each) was then added to the culture. After incubation for 30 min to allow uptake of the amino acids, protein expression was induced by the addition of 0.5 mM IPTG, and the cells were incubated overnight at 25 °C. The proteins were subsequently purified as described above.

### Buffer Solutions for $Zn^{2+}$ Ions

Metal stock solutions were prepared from Zn/HCl atomic absorption standards using 200 mM Bis-Tris and 1 M NaCl stock solutions. Solutions were made in 50 mL volumetric flasks, and pH was adjusted immediately before bringing to volume to minimize dilution effects. All glassware was acid-washed and rinsed thoroughly with 18 MΩ water to eliminate trace metal contamination. All the experiments were performed using 50 mM Bis-Tris with 100 mM NaCl at pH 7.4. Under these conditions, the Bis-Tris−Zn(II) association constant (Ka = 240)[28] predicts that approximately 84.6% of the buffer exists in its deprotonated, metal-binding form. Consequently, roughly 1.63 mM of Zn(II) is chelated by Bis-Tris, accounting for ∼90.6% of the total metal in the 5 mM solution Zn(II) stock solution (50 mM Bis-Tris, 100 mM NaCl, pH 7.4). This high degree of buffer coordination stabilizes the Zn(II) stock solution, which remains free of precipitate for several months.[29,30]

### Aggregation Kinetics

To investigate the kinetics of TTR aggregation in the presence of $Zn^{2+}$ ions, optical density at 400 nm was measured using UV-Vis spectroscopy (ThermoScientific Evolution 201 UV-Vis Spectrophotometer). Kinetic experiments were conducted with TTR at a concentration of 0.25 mg/mL in the presence of varying concentrations of $Zn^{2+}$ ions at pH 7.4 (50 mM Bis-Tris with 100 mM NaCl). Samples were prepared in triplicate for each condition and measured over 8−10 h, with constant agitation (250 rpm) at 37°C. Optical aggregation assays, which are more sensitive to the formation of non-fibrillar TTR aggregates than thioflavin T (ThT) fluorescence, have been used for TTR aggregation.[9,20,21]

### Isothermal Titration Calorimetry (ITC)

All ITC measurements were performed at 25 °C using a MicroCal VP-ITC Ultrasensitive Titration Calorimeter. Titrations were performed in (at least) triplicate to ensure measurement reproducibility and statistical significance. The metal (titrant) and protein (titrand) stocks in 50 mM Bis-Tris with 100 mM NaCl were diluted with identical buffer solutions to final metal and protein concentrations of 0.5−1.5 mM and 27−55 μM, respectively. The sample cell containing the titrand was stirred at 307 rpm to ensure rapid mixing. A typical experiment included 8−10 μL of metal delivered to the sample cell over a 16−20 second period, followed by a 300-second stirring period to ensure a return to baseline. Titrations were continued until approximately 5-7 molar equivalents of metal were added to the sample, ensuring complete saturation of the protein. For each experiment, the last ten data points were averaged and subtracted from the titration curve to account for the heat of dilution. This study utilized the 7.0 Origin® software package (provided by MicroCal) to fit the integrated ITC data.

### Negative-Stain Transmission Electron Microscopy (TEM)

Carbon-coated Formvar 300-mesh copper grids were glow-discharged for 30 s using a PELCO easiGlow system prior to sample application. A 5 μL aliquot of the oligomer preparation was deposited onto the activated grids and allowed to adsorb for 30 s. Excess sample was removed by gentle blotting with filter paper. The grids were rinsed with 30 μL droplets of distilled water, followed by a brief wash in 30 μL droplets of 2% uranyl formate. Negative staining was performed by incubating the grids on a fresh 30 μL droplet of 2% uranyl formate for 30 s. Excess stain was carefully blotted away, and the grids were allowed to air-dry before imaging. Micrographs were acquired using a Talos L120C transmission electron microscope operated at an accelerating voltage of 120 kV.

### Toxicity (MTT Assay)

For toxicity experiments, MTT cell viability assays were employed (CyQuant MTT Cell Viability Assay) in accordance with suggested protocol. SH-SY5Y neuroblastoma cells were cultured in a DMEM/F12 medium in a humidified atmosphere at 37 °C (DMEM/F12, 1% Pen-Strep 10% FBS, and 5% $CO_2$). The growth medium was replaced every 5 days until reaching a cell density of 10,000 cells per well and plating in a 96 well plate. The mammalian cells were allowed to settle on the plate for 24 h before renewing the medium with 200 μL of fresh DMEM/F12 medium containing TTR at different concentrations. The cells were incubated for 48 h before removing the medium and replacing with 100 μL of fresh medium and treating with MTT. After an additional 4 h incubation period, 100 μL of sodium dodecyl sulfate hydrochloric acid (SDS-HCl) was added to each well before further incubation for 4 h. The optical density was then recorded at 570 nm using a microplate reader (SpectraMax®). Each condition for MTT assay was prepared and measured in triplicate.

### Solution NMR

Two-dimensional (2D) $^{1}H-^{15}N$ heteronuclear single-quantum coherence (HSQC) NMR spectra were acquired at 25 °C on a Bruker 850 MHz spectrometer equipped with a cryogenic $^{1}H/^{13}C/^{15}N$ triple-resonance probe, using the transverse relaxation-optimized spectroscopy (TROSY) pulse sequence.[31] Complex data points of 2048 × 256 were collected for all the samples, and 128 FIDs

Downloaded from pubs.acs.org/biochaw/article-pdf/65/19/3017/6854085/acs.biochem.6c00448.pdf by FLORIDA STATE UNIV user on 02 November 2026


https://doi.org/10.1021/acs.biochem.6c00448
Biochemistry 2026, 65, 3017−3025

were accumulated for each t1 data point with an acquisition delay of 2 s. Topspin 4.5 and NMRviewJ[32] were used to process and analyze the NMR data.

The $^{19}F$ NMR spectra were acquired without $^{1}H$ decoupling on a Bruker 500 MHz NMR spectrometer equipped with a cryogenic $^{1}H-^{19}F/^{13}C/^{15}N$ probe. Free induction decays (FIDs) were collected with 8K complex data points over a spectral width of 30 ppm and zero-filled to 64K prior to Fourier transformation. A 20 Hz line-broadening function was applied before Fourier transformation.

### Solid-State NMR

Two-dimensional (2D) $^{13}C-^{13}C$ solid-state NMR spectra were recorded at 25°C using a Bruker 800 MHz NMR spectrometer equipped with a home-built 3.2 mm MAS $^{1}H/^{13}C/^{15}N$ probe at the National High Magnetic Field Laboratory (NHMFL). The 90° pulse lengths were 3.2 $\mu$s for $^{1}H$ and 5.5 $\mu$s for $^{13}C$. A dipolar-assisted rotational resonance (DARR)[33] mixing scheme with a mixing time of 20 ms was used for the 2D experiments at a magic-angle spinning (MAS) rate of 13 kHz. A SPINAL-64 decoupling scheme[34] was applied during detection with an $^{1}H$ radiofrequency (rf) power of 80 kHz. Complex data points of 1700 × 640 were collected with 96 FIDs accumulated per $t_1$ data at an acquisition delay of 2 s. NMR data were processed and analyzed using TopSpin 4.5 and NMRViewJ.[35]

## RESULTS

The aggregation kinetics of TTRwt was first examined, with optical density (OD) measured at 400 nm in the presence of the metal ions (Figure 1). The natively folded TTRwt is highly stable at the physiological conditions (pH of 7.4 and concentrations of 0.2−0.4 mg/mL) and no aggregation was observed in the absence of the metal ions. The aggregation kinetics of TTRwt at varying $Zn^{2+}$ concentrations demonstrated that these metal ions accelerate the misfolding and aggregation of TTRwt (Figure 1a).

Transmission electron microscopy (TEM) was employed to investigate the morphology of metal-induced TTR aggregates (Figure 1b), revealing less ordered aggregate structures. Notably, dilution of the TTR aggregates produces small oligomeric species, suggesting that $Zn^{2+}$ induces the formation of oligomeric aggregates (Figure 1c). The cytotoxicity and seeding activity of the misfolded oligomers were subsequently examined. Cytotoxic effects were evaluated using a 3-(4,5-dimethylthiazol-2-yl)-2,5-diphenyltetrazolium bromide (MTT) assay (Figure S1). The viability assay shows that $Zn^{2+}$-induced TTRwt oligomers are more toxic than native TTRwt.

Kinetic experiments were performed in the presence and absence of preformed TTR aggregates to investigate whether $Zn^{2+}$-induced oligomers promote TTRwt aggregation under both $Zn^{2+}$-free and $Zn^{2+}$-containing conditions (Figure 2). Preformed TTRwt aggregates clearly promoted further aggregation even in the absence of $Zn^{2+}$ (blue versus orange traces). Aggregation was further accelerated in the presence of $Zn^{2+}$ (purple versus red), demonstrating that $Zn^{2+}$-induced oligomeric aggregates are capable of seeding TTR misfolding and aggregation.

The metal ion binding was investigated using isothermal titration calorimetry (ITC) (Figure S2). $Zn^{2+}$ was titrated into TTRwt (0.2 mg/mL; 15 $\mu$M monomer concentration) up to a TTR/$Zn^{2+}$ ratio of 1:5 in 50 mM bis-tris buffer (pH 7.4). Three independent ITC experiments were performed under identical conditions. A representative titration is shown in Figure S2a, displaying the differential power signal measured for each injection and the resulting isotherm (Figure S2b). The ITC isotherm clearly demonstrates effective binding of $Zn^{2+}$ to TTRwt.

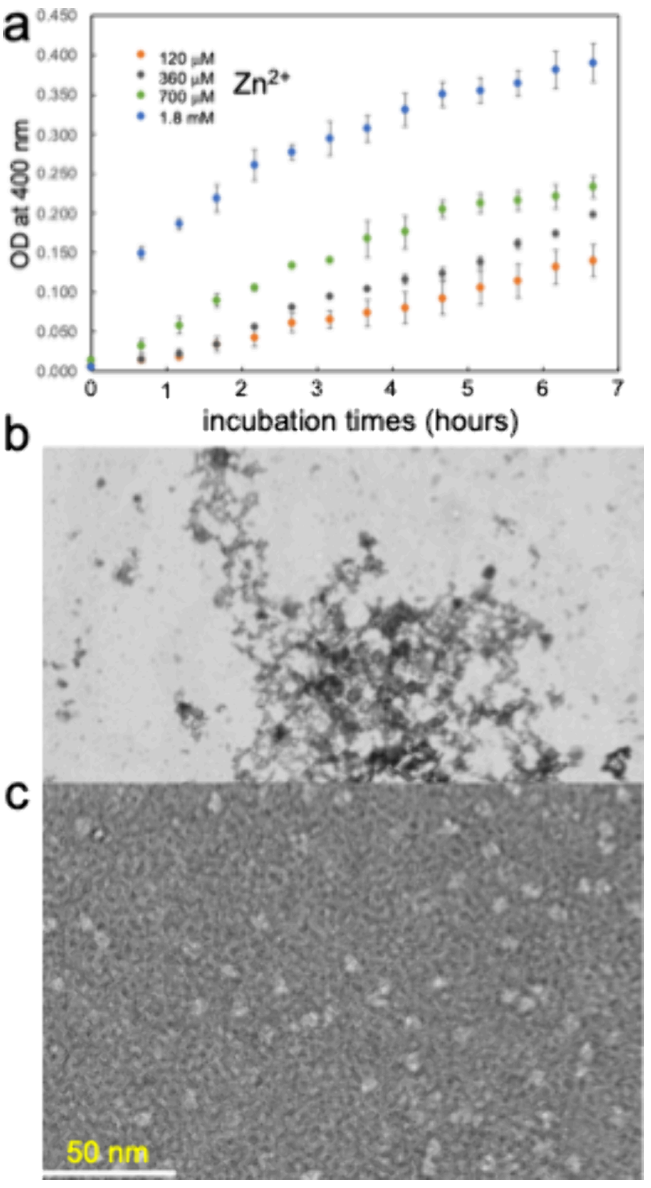



**Figure 1.** (a) Aggregation kinetics of TTRwt (0.4 mg/mL, 30 $\mu$M monomer concentration) at pH 7.4 in the presence of $Zn^{2+}$ ions with different concentrations. (b) TEM image of $Zn^{2+}$-induced TTRwt aggregates obtained at a protein concentration of 2 mg/mL. (c) TEM image of $Zn^{2+}$-induced TTRwt aggregates obtained after 100 × dilution. The errors in (a) were calculated from the three experiments and the error bars for many of the data points are smaller than the size of the marker. In the 1.8 mM $Zn^{2+}$ solution, the concentration of free $Zn^{2+}$ is estimated to be 0.25 mM based on the association constant of 240 (Buffer solutions in the Materials and Method section).

The structural features of the metal-induced oligomers were investigated using solid-state NMR spectroscopy (Figure 3). Two-dimensional (2D) $^{13}C-^{13}C$ and $^{15}N-^{13}C\alpha$ correlation solid-state NMR spectroscopy is well suited for comparative structural analyses of aggregates at the molecular level, as $^{13}C$ chemical shifts of aliphatic carbons are highly sensitive to secondary structure, while $^{15}N$ chemical shifts report on hydrogen-bonding geometry.[36,37] The 2D $^{13}C-^{13}C$ NMR spectra obtained using a dipolar-assisted rotational resonance (DARR) mixing scheme[33] show that the NMR cross-peaks from the metal-induced TTRwt aggregates (red) overlap well with those of native TTR (blue) (Figure 3a and Figure S3),

Downloaded from pubs.acs.org/bichaw/article-pdf/65/19/3017/6854085/acs.biochem.6c00448.pdf by FLORIDA STATE UNIV user on 02 November 2026


https://doi.org/10.1021/acs.biochem.6c00448
Biochemistry 2026, 65, 3017−3025

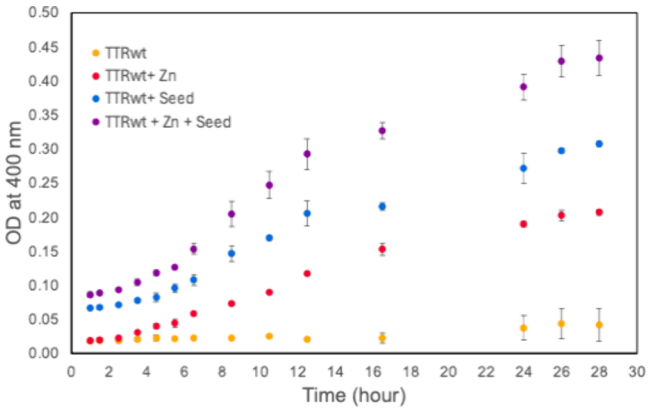



**Figure 2.** Aggregation kinetics of TTRwt (2 mg/mL) at pH 7.4 in the absence and presence of $Zn^{2+}$ (1:1 ratio) and preformed $Zn^{2+}$-induced TTRwt aggregates (5 %). The $Zn^{2+}$-induced aggregates used as seeds were washed three times by repeated resuspension and centrifugation cycles using 50 mM bis-tris buffer to remove free $Zn^{2+}$ from the solution.

suggesting that most native-like $\beta$-sheet secondary structures are preserved in the aggregates. Notably, some cross-peaks present in native TTR were shifted or absent in the aggregate spectrum, while most of the peaks remained unchanged. Resonance assignments from our previous 3D solid-state NMR experiments,[38] indicate that the resonances from strand H (residues 115−123) at the dimeric interface are absent in the aggregates (Figure 3a and Figure S4). This suggests that aggregation-prone species dissociated from the native tetramer self-assemble into larger aggregates (Figure 3a). On the other hand, the distinct 2D NCA spectrum of the oligomers compared with that of native TTR clearly indicates that the $Zn^{2+}$-induced oligomers adopt non-native conformations (Figure 3b).

Previous NMR studies suggested that the $Zn^{2+}$-binding sites of TTRwt may have different binding affinities based on the chemical shift changes.[39] It is, therefore, important to investigate which binding interactions are responsible for misfolding and aggregation. Two-dimensional (2D) $^{1}H/^{15}N$ HSQC NMR spectra were acquired at higher TTR/$Zn^{2+}$ ratios than those used in previous studies, in order to probe TTR−$Zn^{2+}$ interactions that may contribute to misfolding (Figure 4a and Figure S5). The overlaid HSQC spectra acquired at

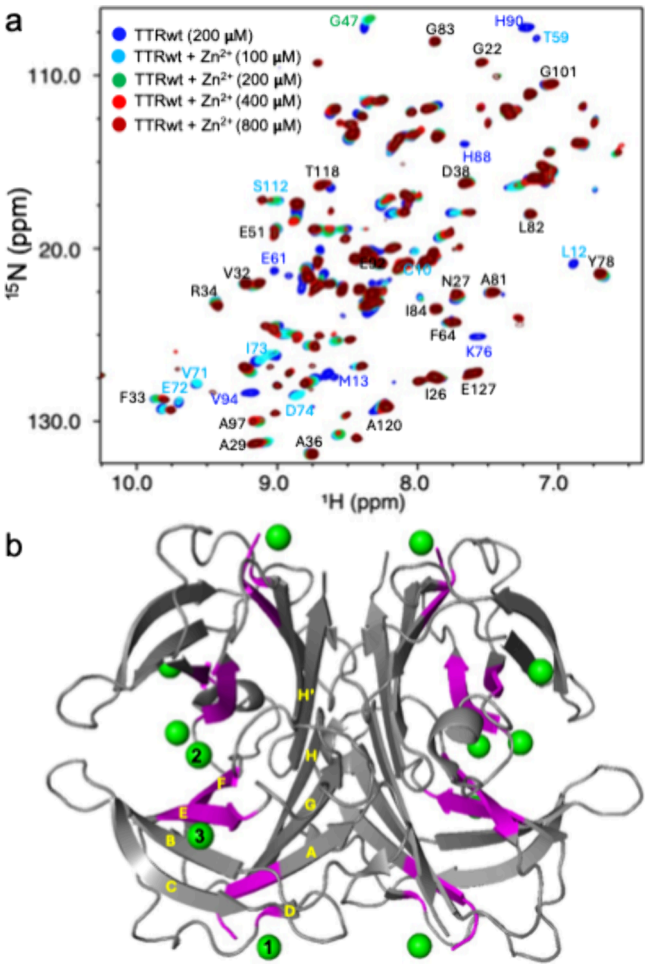



**Figure 4.** (a) Overlaid 2D $^{1}H/^{15}N$ TROSY-HSQC NMR spectra of TTRwt (200 $\mu$M, monomer concentration) in the absence and presence of $Zn^{2+}$ at pH 7.4 and 25 °C acquired using 850 MHz NMR. (b) A ribbon diagram representation of TTRwt tetramer showing residues (pink) affected by $Zn^{2+}$ in Figure 4a.

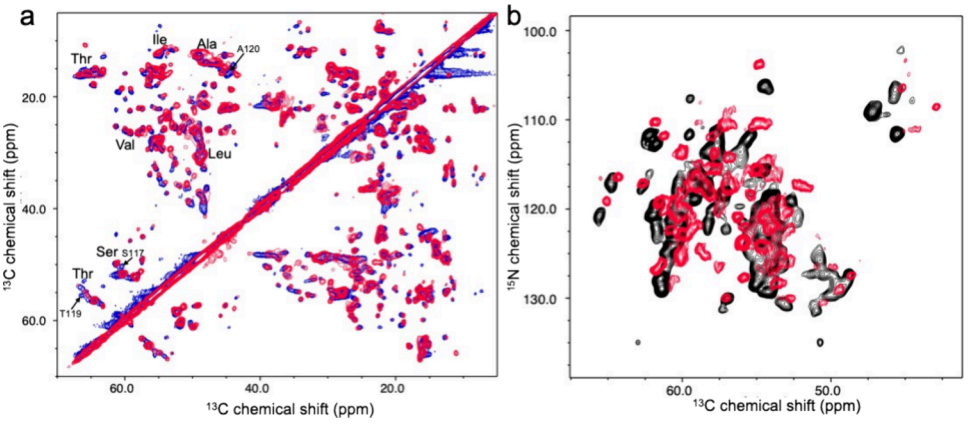



**Figure 3.** (a) Aliphatic regions of the $^{13}C$-detected 2D solid-state NMR DARR spectra for the native (blue) and $Zn^{2+}$-induced TTRwt (red) acquired using 800 MHz NMR. A DARR mixing time of 20 ms was used for the 2D NMR spectra. (b) An overlaid 2D NCA spectra of the native TTRwt (black) and $Zn^{2+}$-induced TTRwt oligomers (red). The metal-induced aggregates were packed into 3.2 mm MAS rotors by centrifugation. The aggregates inside the rotor have remained stable, reproducing the identical spectra.



https://doi.org/10.1021/acs.biochem.6c00448
Biochemistry 2026, 65, 3017−3025

Downloaded from pubs.acs.org/biochaw/article-pdf/65/19/3017/6854085/acs.biochem.6c00448.pdf by FLORIDA STATE UNIV user on 02 November 2026

different TTR/$Zn^{2+}$ ratios (brown) revealed that about 30 % of the cross-peaks gradually disappeared, while 70 % of the peaks remain unchanged. Similar behaviors were observed at a lower TTR concentration of 70 $\mu$M (Figure S6), indicating that the line-broadening is likely due to conformational fluctuations on millisecond (ms) time scales, rather than intermolecular interactions. In addition, the similar line-broadening was also observed at a higher TTR/$Zn^{2+}$ ratio in which TTR is nearly fully saturated (Figure S7), supporting the internal conformational exchanges.

Backbone assignment of the cross-peaks that were made based on the previous backbone assignments (BMRB 5507 and 27514)[40,41] and 3D HNCA experiment revealed that the residues affected by $Zn^{2+}$ ions are mostly located in the binding sites determined by X-ray crystallography (Figure 4b and Figure S8). The binding sites are almost uniformly, though not identically, affected by the metal ions, suggesting that conformational fluctuations across all binding sites may play a critical role in the misfolding transition. In contrast, most residues in the other CB and GH $\beta$-sheets remain unaffected.

Recent studies have shown that fluorinated Trp residues (F6-Trp-TTR, Figure 5a) can be incorporated into TTR without affecting its native structure or misfolding properties.[42] Our 2D $^{1}H/^{15}N$ HSQC NMR experiments further confirm that the native TTR structure remains unchanged upon fluorination of the side chain (Figure 5b). In addition, one of the two Trp residues, W41, is located near the $Zn^{2+}$-binding site (Figure 5c), potentially allowing us to probe $Zn^{2+}$-induced structural and dynamical changes in TTR.

The effect of the metal ion binding was investigated by $^{19}F$ NMR using F6-Trp-TTR (Figure 6). Upon the addition of $Zn^{2+}$, the NMR resonance from residue W41 is notably broadened, suggesting that the metal ions induce conformational fluctuations on millisecond time scales (Figure 6a) consistent with the $^{1}H/^{15}N$ HSQC results. Notably, a new resonance upfield shifted by 0.6 ppm appeared at lower temperatures (Figure 6b). It was previously shown that cold-induced disruption of interfacial water perturbs the hydration network at the subunit interfaces.[43] At lower temperatures, this disruption may, therefore, destabilize the TTR tetramer, promoting its dissociation into dimers and monomers and thereby facilitating subunit exchange. In addition, the new resonance becomes stronger in intensity compared to that of tetramers at a lower TTR concentration (* in Figure 6c). Previous $^{19}F$ NMR studies employing a strategically placed trifluoroacetyl probe revealed that TTR dissociation to monomers is promoted at lower temperatures and lower TTR concentration,[20,21] strongly suggesting that the new resonance comes from monomeric intermediate states that form during the misfolding transition.

The $Zn^{2+}$ titration experiments performed at a low temperature (277 K) further confirm the effects of $Zn^{2+}$ binding (Figure 7). Initial $Zn^{2+}$ binding appears to induce conformational changes around W41, as evidenced by significant line broadening of the W41 resonance. At higher TTR:$Zn^{2+}$ ratios (>1:4), the new resonance emerges and increases in intensity, suggesting dissociation of the native tetrameric structure. At a lower protein concentration, the new resonance becomes stronger in intensity, confirming the dissociation of native tetramers (Figure S9). The dissociation of the tetramer appears to alter the local environment of the W41 side chain (Figure 5c), resulting in the observed chemical-shift change. Interestingly, the W79 resonance is

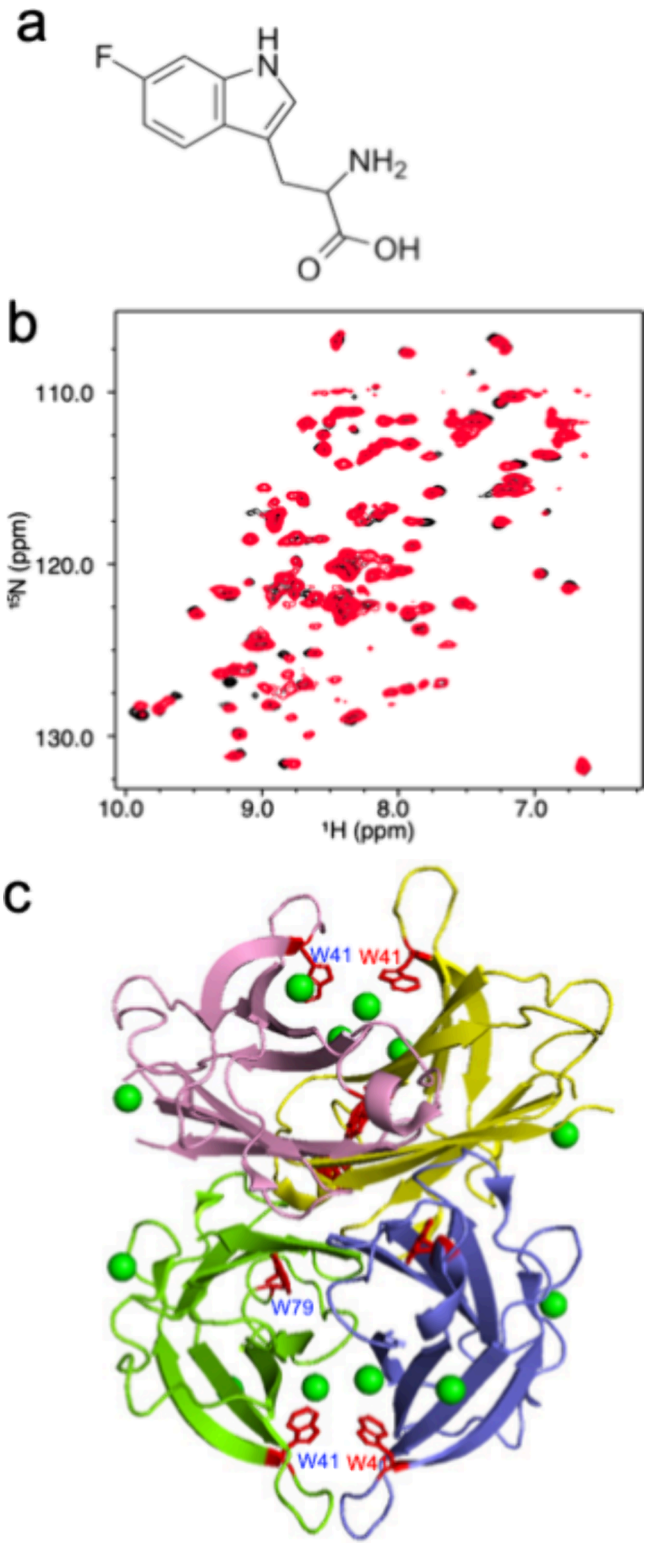



**Figure 5.** (a) 6-Fluoro-tryptophan. (b) Overlaid 2D $^{1}H/^{15}N$ HSQC spectra for the native TTRwt (black) and F6-Trp-TTRwt (red) at 298 K. (c) X-ray crystal structure of TTRwt with metal ions, $Zn^{2+}$ (green, 3grg).[39] The two NMR spectra are nearly identical, suggesting that incorporation of F6-Trp into TTR dose not affect the structure.

only minimally affected by $Zn^{2+}$ addition, exhibiting only slight line broadening (Table 1). Although W79 is located near the dimer−dimer interface, its side chain is largely buried within the hydrophobic core of the TTR monomer (Figure 5c). The

Downloaded from pubs.acs.org/bichaw/article-pdf/65/19/3017/6854085/acs.biochem.6c00448.pdf by FLORIDA STATE UNIV user on 02 November 2026


https://doi.org/10.1021/acs.biochem.6c00448
Biochemistry 2026, 65, 3017−3025

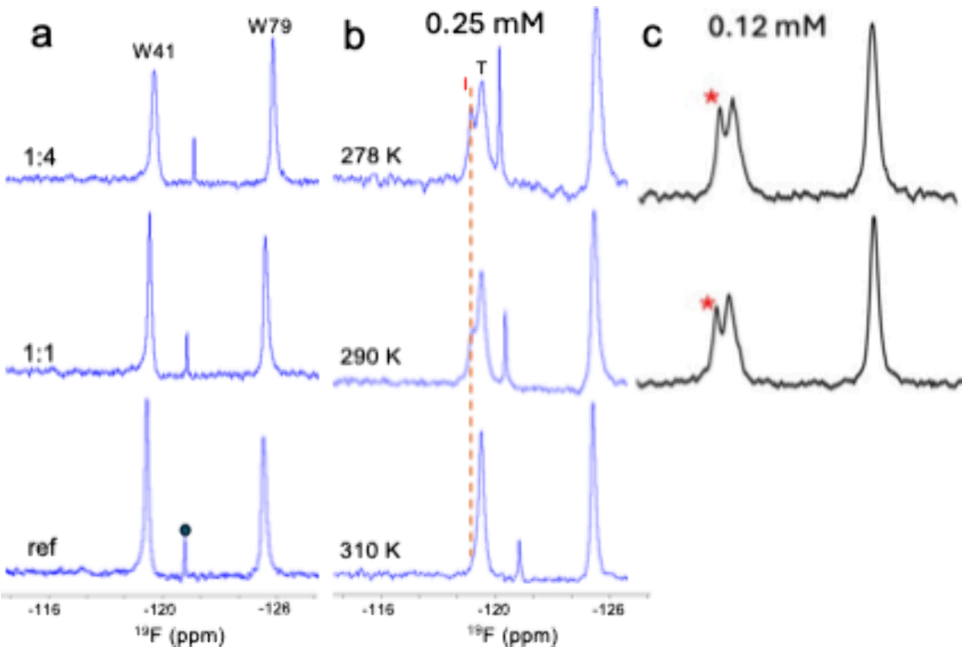



**Figure 6.** (a) $^{19}$F solution NMR spectra of F6-Trp-TTRwt at different TTR/$Zn^{2+}$ ratios at 310 K. (b) $^{19}$F NMR spectra of the TTR/$Zn^{2+}$ complex (1:8) at different temperatures using a TTR concentration of 0.25 mM. (c) $^{19}$F NMR spectra of the TTR/$Zn^{2+}$ complex using a TTR concentration of 0.12 mM. The NMR spectra were averaged over 500−2000 scans with a 1s recycle delay. The peak marked by circle in (a) is from free fluoride ions from the NMR tube.[44]

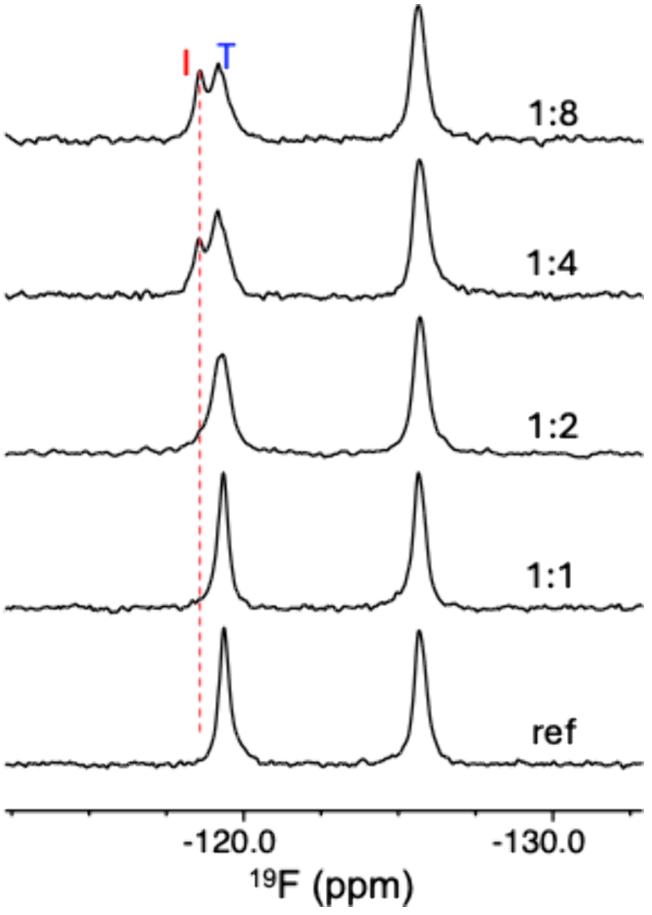



**Figure 7.** $^{19}$F solution NMR spectra of F6-Trp-TTRwt at different TTR:$Zn^{2+}$ ratios at 277 K. The NMR tubes were extensively washed with buffer to remove the $F^-$ ions from the NMR tube.

**Table 1. Line Width of the $^{19}$F NMR Resonances at Different TTR/$Zn^{2+}$ Ratios in Figure 7**

| TTR:$Zn^{2+}$ ratio | W41 (ppm) | W79 (ppm) |
|---|---|---|
| ref | 0.35 | 0.44 |
| 1:1 | 0.35 | 0.43 |
| 1:2 | 0.63 | 0.48 |
| 1:4 | | 0.52 |
| 1:8 | | 0.55 |

limited perturbation of the W79 resonance suggests that the monomers generated upon tetramer dissociation remain largely folded and retain a native-like local structure around W79 side chain.

## DISCUSSION

Physiological metal ions play important roles in diverse biological functions, such as maintaining cellular homeostasis, facilitating enzyme activity, stabilizing protein structures, and regulating signaling pathways. Metal ions like $Ca^{2+}$ and $Zn^{2+}$ can influence conformational stability and dynamics, potentially accelerating misfolding and aggregation processes.[17] Indeed our biophysical analyses revealed that metal ions ($Zn^{2+}$) accelerate TTR misfolding and aggregation. Although physiological $Zn^{2+}$ concentration in serum is 12−15 $\mu$M,[45] it was previously shown that the cellular zinc concentration can fluctuate in response to various stimuli, and the zinc concentration can be up to hundreds of micromolar.[46] In addition, elevated levels of these metal ions have been observed in ex vivo TTR aggregates,[18] suggesting that the metal-induced misfolding and aggregation of TTR may take place in vivo based on our experimental conditions (pH, concentrations of TTR and the metal ions in Figure 1) similar to the physiological conditions (TTR concentration of 0.2−0.4 mg/mL).[47]



https://doi.org/10.1021/acs.biochem.6c00448
Biochemistry 2026, 65, 3017−3025

Downloaded from pubs.acs.org/bichaw/article-pdf/65/19/3017/6854085/acs.biochem.6c00448.pdf by FLORIDA STATE UNIV user on 02 November 2026

Previous structural studies of $Zn^{2+}$-TTR complex using X-ray crystallography identified three $Zn^{2+}$ ions binding sites within the tetramer (Figure 5c).[39] However, the binding sites were determined by crystallizing the monomeric variant (F87M/L110M, M-TTR; 0.9 mM) in the presence of excessive amounts of $Zn^{2+}$ ions (200 mM), which may not reflect physiological conditions. Previous chemical shift perturbation analysis using $^{1}H/^{15}N$ HSQC NMR experiments revealed that the three binding sites are not equally affected ($1 \gg 2 \approx 3$ in Figure 3b), suggesting that the binding sites may have different affinities.[39] It was also reported that the HN resonances are broadened at higher $Zn^{2+}$ concentrations in the 2D HSQC NMR spectra, indicative of conformational exchange processes occurring on the microsecond to millisecond ($\mu$s−ms) time scale.[39] However, only chemical shift changes were analyzed to examine the effect of the metal ion binding and the broader impact of metal ion binding on the misfolding pathway remained largely unexplored.

Our NMR studies were conducted at lower TTR concentrations (0.070−0.2 mM monomer concentration) with a wider range of TTR/Zn ratios (0.5−4) (Figure 4a and Figure S7) compared to the previous NMR experimental conditions (0.4 mM TTR and 0.1−0.9 mM $Zn^{2+}$). Significant line broadening was clearly observed in the NH resonances at both TTR concentrations, suggesting that TTR undergoes conformational exchanges on the ms time scale upon $Zn^{2+}$ binding, which was also observed in $^{19}F$ NMR (Figure 6a and 7). Notably, the three binding sites were affected in a nearly uniform manner, albeit not identically, (Figure S8) suggesting that $Zn^{2+}$ binding at all three sites is required for effective conformational changes leading to non-native oligomers.

It is also interesting to note that resonances at the dimeric and tetrameric interfaces in the native state remain unaffected by initial metal ion binding, indicating that the conformational exchanges occur primarily among the monomers within the tetrameric assembly (Figure 4b and S10). Our $^{19}F$ NMR also confirms the conformational fluctuations of the monomer subunit within the tetramers upon initial $Zn^{2+}$ bindings (Figure 7). These results suggest that the metal ions initially destabilize the conformations of the monomeric subunits within the tetramer, consistent with previous urea-denaturation studies demonstrating that TTR monomers are more susceptible to metal ion-induced destabilization than the tetrameric state.[39]

Dissociation of the tetramer was observed at lower temperatures in the presence of $Zn^{2+}$ (Figure 6 and 7), and this effect became more pronounced at a lower protein concentration (Figure 6c and S9). These results indicate that $Zn^{2+}$ binding initially induces conformational fluctuations within the tetrameric assembly, which subsequently promotes tetramer dissociation into monomers (Figure S10). These monomeric species then undergo self-association to form oligomeric assemblies.

Previous studies have shown that TTR assemblies formed under mildly acidic conditions are unable to trigger TTR misfolding and aggregation.[48] In contrast, ex vivo TTR aggregates were shown to effectively promote TTR aggregation,[49] suggesting that these *ex vivo* aggregates possess structural characteristics required for seeding activity. Notably, $Zn^{2+}$-induced TTR oligomeric aggregates effectively promote aggregation of TTRwt at physiological pH, implying that these oligomers may adopt structural features similar to those of pathogenic TTR aggregates that are competent for seeding.

## CONCLUSION

In summary, we demonstrate that $Zn^{2+}$ ions induce the formation of toxic, seeding-competent oligomers under physiological conditions. Our combined analyses using 2D $^{1}H/^{15}N$ and $^{19}F$ NMR revealed that $Zn^{2+}$ binding promotes local conformational perturbations within the tetrameric assembly, accelerating its dissociation into aggregation-prone monomers that subsequently self-assemble into the oligomeric aggregates. These combined NMR analyses would provide a framework for elucidating the molecular basis of $Zn^{2+}$-induced misfolding and aggregation of diverse pathogenic TTR variants associated with distinct disease phenotypes under physiologically relevant conditions. The $^{19}F$ NMR would be a particularly useful tool to probe not only initial $Zn^{2+}$ binding but also tetramer dissociation into monomers.

## ASSOCIATED CONTENT

### Supporting Information

The Supporting Information is available free of charge at https://pubs.acs.org/doi/10.1021/acs.biochem.6c00448.

Toxicity results. ITC binding isotherm. NMR assignment of the native DARR spectrum. 2D $^{1}H/^{15}N$ HSQC NMR spectra at a lower TTR concentration. One-dimensional slices of the 2D spectra. Intensity change profile upon $Zn^{2+}$ binding. Proposed mechanism of $Zn^{2+}$ induced-misfolding and aggregation of TTR. (PDF)

### Accession Codes

Accession Codes Transthyretin: UniProtKB entry P02766.

## AUTHOR INFORMATION


### Corresponding Author

**Kwang Hun Lim** − *Department of Chemistry, East Carolina University, Greenville, North Carolina 27858, United States;* orcid.org/0000-0002-0971-200X; Email: limk@ecu.edu

### Authors

**Robert Irving** − *Department of Chemistry, East Carolina University, Greenville, North Carolina 27858, United States;* orcid.org/0009-0004-8506-3728

**Anvesh Dasari** − *Electron Microscopy Shared Resources, Fred Hutchinson Cancer Center, Seattle, Washington 98109, United States*

**Sy Duke** − *Department of Chemistry, East Carolina University, Greenville, North Carolina 27858, United States*

**Sungsool Wi** − *Interdisciplinary Magnetic Resonance (CIMAR), National High Magnetic Field Laboratory (NHMFL), Tallahassee, Florida 32310, United States;* orcid.org/0000-0003-0728-095X

**Robert M. Hughes** − *Department of Chemistry, East Carolina University, Greenville, North Carolina 27858, United States;* orcid.org/0000-0002-4465-4212

**Anne M. Spuches** − *Department of Chemistry, East Carolina University, Greenville, North Carolina 27858, United States*

Complete contact information is available at: https://pubs.acs.org/10.1021/acs.biochem.6c00448


### Author Contributions

R.I. and S.D. prepared the protein samples. R. H. conducted toxicity test, and A.K.R.D. and S. W. acquired TEM images and solid-state NMR spectra, respectively. A.M.S. performed ITC

Downloaded from pubs.acs.org/biochaw/article-pdf/65/19/3017/6854085/acs.biochem.6c00448.pdf by FLORIDA STATE UNIV user on 02 November 2026

experiments. K.H.L. designed and analyzed the experimental data. R.I., A.K.R.D., R.H. A.M.S. and K.H.L. wrote the manuscript.

### Funding

This work was funded by NIH grant (GM163276) to K.H.L., and the National High Magnetic Field Laboratory is supported by the State of Florida and the National Science Foundation through NSF/DMR-1644779. The solution NMR studies were also supported by the National Cancer Institute of the NIH under award number P30CA016086.

### Notes

The authors declare no competing financial interest.

## ■ ACKNOWLEDGMENTS

The authors acknowledge Dr. Parnham at UNC at Chapel Hill for assistance with NMR data collection.

## ■ ABBREVIATIONS

| | |
|---|---|
| NMR | nuclear magnetic resonance |
| DARR | dipolar assisted rotational resonance |
| TTR | transthyretin |
| TTRwt | wild-type WT |
| TEM | transmission electron microscopy |
| HSQC | heteronuclear single-quantum coherence |
| MAS | magic-angle spinning |
| MTT | 3-(4,5-dimethylthiazol-2-yl)-2,5-diphenyltetrazolium bromide |
| ATTR | TTR amyloidosis |
| OD | optical density |
| DARR | dipolar-assist rotational resonance |

## ■ REFERENCES

(1) Buxbaum, J. N.; Reixach, N. Transthyretin: The servant of many masters. *Cell Mol. Life Sci.* **2009**, *66*, 3095−3101.
(2) Herbert, J.; Wilcox, J. N.; Pham, K. T.; Fremeau, R. T., Jr; Zeviani, M.; Dwork, A.; Soprano, D. R.; Makover, A.; Goodman, D. S.; Zimmerman, E. A.; et al. Transthyretin: A choroid plexus-specific transport protein in human brain. the 1986 S. weir mitchell award. *Neurology* **1986**, *36*, 900−911.
(3) Sacchettini, J. C.; Kelly, J. W. Therapeutic strategies for human amyloid diseases. *Nat. Rev. Drug Discovery* **2002**, *1*, 267−275.
(4) Ruberg, F. L.; Grogan, M.; Hanna, M.; Kelly, J. W.; Maurer, M. S. Transthyretin amyloid cardiomyopathy: JACC state-of-the-art review. *J. Am. Coll. Cardiol.* **2019**, *73*, 2872−2891.
(5) Westermark, P.; Sletten, K.; Johansson, B.; Cornwell, G. G. Fibril in senile systemic amyloidosis is derived from normal transthyretin. *Proc. Natl. Acad. Sci. U.S.A.* **1990**, *87*, 2843−2845.
(6) Coelho, T.; Maurer, M. S.; Suhr, O. B. THAOS - the transthyretin amyloidosis outcomes survey: Initial report on clinical manifestations in patients with hereditary and wild-type transthyretin amyloidosis. *Curr. Med. Res. Opin.* **2013**, *29*, 63−76.
(7) Westermark, P.; Bergstrom, J.; Solomon, A.; Murphy, C.; Sletten, K. Transthyretin-derived senile systemic amyloidosis: Clinicopathologic and structural considerations. *Amyloid* **2003**, *10* (Suppl 1), 48−54.
(8) Herrick, M. K.; DeBruyne, K.; Horoupian, D. S.; Skare, J.; Vanefsky, M. A.; Ong, T. Massive leptomeningeal amyloidosis associated with a Val30Met transthyretin gene. *Neurology* **1996**, *47*, 988−992.
(9) Lai, Z. H.; Colon, W.; Kelly, J. W. The acid-mediated denaturation pathway of transthyretin yields a conformational intermediate that can self-assemble into amyloid. *Biochemistry* **1996**, *35*, 6470−6482.
(10) Lashuel, H. A.; Lai, Z. H.; Kelly, J. W. Characterization of the transthyretin acid denaturation pathways by analytical ultracentrifugation: Implications for wild-type, V30M, and L55P amyloid fibril formation. *Biochemistry* **1998**, *37*, 17851−17864.
(11) Quintas, A.; Vaz, D. C.; Cardoso, I.; Saraiva, M. J.; Brito, R. M. Tetramer dissociation and monomer partial unfolding precedes protofibril formation in amyloidogenic transthyretin variants. *J. Biol. Chem.* **2001**, *276*, 27207−27213.
(12) Tamás, M. J.; Sharma, S. K.; Ibstedt, S.; Jacobson, T.; Christen, P. Heavy metals and metalloids as a cause for protein misfolding and aggregation. *Biomolecules* **2014**, *4*, 252−267.
(13) Wang, L.; Yin, Y.; Liu, X.; Shen, P.; Zheng, Y.; Lan, X.; Lu, C.; Wang, J. Current understanding of metal ions in the pathogenesis of alzheimer's disease. *Translational Neurodegeneration* **2020**, *9*, 10.
(14) Byrd, E. J.; Wilkinson, M.; Radford, S. E.; Sobott, F. Taking charge: Metal ions accelerate amyloid aggregation in sequence variants of α-synuclein. *J. Am. Soc. Mass Spectrom.* **2023**, *34*, 493−504.
(15) Moons, R.; Konijnenberg, A.; Mensch, C.; Van Elzen, R.; Johannessen, C.; Maudsley, S.; Lambeir, A.; Sobott, F. Metal ions shape α-synuclein. *Sci. Rep.* **2020**, *10*, 16293.
(16) Suh, J.; Kim, M.; Yoo, J.; Han, J.; Paulina, C.; Lim, M. H. Intercommunication between metal ions and amyloidogenic peptides or proteins in protein misfolding disorders. *Coord. Chem. Rev.* **2023**, *478*, 214978.
(17) Wilkinson-White, L.; Easterbrook-Smith, S. Characterization of the binding of cu(II) and zn(II) to transthyretin: Effects on amyloid formation. *Biochemistry (N. Y. )* **2007**, *46*, 9123−9132.
(18) Susuki, S.; Ando, Y.; Sato, T.; Nishiyama, M.; Miyata, M.; Suico, M. A.; Shuto, T.; Kai, H. Multi-elemental analysis of serum and amyloid fibrils in familial amyloid polyneuropathy patients. *Amyloid* **2008**, *15*, 108−116.
(19) Thelander, U.; Westermark, G. T.; Antoni, G.; Estrada, S.; Zancanaro, A.; Ihse, E.; Westermark, P. Cardiac microcalcifications in transthyretin (ATTR) amyloidosis. *Int. J. Cardiol.* **2022**, *352*, 84−91.
(20) Sun, X.; Dyson, H. J.; Wright, P. E. Kinetic analysis of the multistep aggregation pathway of human transthyretin. In *Proceedings of the National Academy of Sciences*, 2018; Vol. *115*, pp E6201−E6208.
(21) Sun, X.; Ferguson, J. A.; Leach, B. I.; Stanfield, R. L.; Dyson, H. J.; Wright, P. E. Probing the dissociation pathway of a kinetically labile transthyretin mutant. *J. Am. Chem. Soc.* **2024**, *146*, 532−542.
(22) Larda, S. T.; Simonetti, K.; Al-Abdul-Wahid, M. S.; Sharpe, S.; Prosser, R. S. Dynamic equilibria between monomeric and oligomeric misfolded states of the mammalian prion protein measured by 19F NMR. *J. Am. Chem. Soc.* **2013**, *135*, 10533−10541.
(23) Suzuki, Y.; Brender, J. R.; Soper, M. T.; Krishnamoorthy, J.; Zhou, Y.; Ruotolo, B. T.; Kotov, N. A.; Ramamoorthy, A.; Marsh, E. N. G. Resolution of oligomeric species during the aggregation of Aβ1−40 using 19F NMR. *Biochemistry (N. Y. )* **2013**, *52*, 1903−1912.
(24) Li, C.; Lutz, E. A.; Slade, K. M.; Ruf, R. A.; Wang, G.; Pielak, G. J. 19F NMR studies of α-synuclein conformation and fibrillation. *Biochemistry (N. Y. )* **2009**, *48*, 8578−8584.
(25) Suzuki, Y.; Brender, J. R.; Hartman, K.; Ramamoorthy, A.; Marsh, E. N. G. Alternative pathways of human islet amyloid polypeptide aggregation distinguished by 19F nuclear magnetic resonance-detected kinetics of monomer consumption. *Biochemistry (N. Y. )* **2012**, *51*, 8154−8162.
(26) Sahoo, B. R.; Cox, S. J.; Ramamoorthy, A. High-resolution probing of early events in amyloid-β aggregation related to alzheimer's disease. *Chem. Commun.* **2020**, *56*, 4627−4639.
(27) Lim, K. H.; Dasari, A. K.; Hung, I.; Gan, Z.; Kelly, J. W.; Wright, P. E.; Wemmer, D. E. Solid-state NMR studies reveal native-like beta-sheet structures in transthyretin amyloid. *Biochemistry* **2016**, *55*, 5272−5278.
(28) Magyar, J. S.; Godwin, H. A. Spectropotentiometric analysis of metal binding to structural zinc-binding sites: Accounting quantitatively for pH and metal ion buffering effects. *Anal. Biochem.* **2003**, *320*, 39−54.

Downloaded from pubs.acs.org/bichaw/article-pdf/65/19/3017/6854085/acs.biochem.6c00448.pdf by FLORIDA STATE UNIV user on 02 November 2026

(29) Grossoehme, N. E.; Spuches, A. M.; Wilcox, D. E. Application of isothermal titration calorimetry in bioinorganic chemistry. *JBIC Journal of Biological Inorganic Chemistry* **2010**, *15*, 1183−1191.
(30) Johnson, R. A.; Manley, O. M.; Spuches, A. M.; Grossoehme, N. E. Dissecting ITC data of metal ions binding to ligands and proteins. *Biochimica et Biophysica Acta (BBA)-General Subjects* **2016**, *1860*, 892−901.
(31) Pervushin, K.; Riek, R.; Wider, G.; Wüthrich, K. Attenuated T 2 relaxation by mutual cancellation of dipole−dipole coupling and chemical shift anisotropy indicates an avenue to NMR structures of very large biological macromolecules in solution. In *Proceedings of the National Academy of Sciences*, 1997; Vol. *94*, pp 12366−12371.
(32) Lee, W.; Tonelli, M.; Markley, J. L. NMRFAM-SPARKY: Enhanced software for biomolecular NMR spectroscopy. *Bioinformatics* **2015**, *31*, 1325−1327.
(33) Takegoshi, K.; Nakamura, S.; Terao, T. 13C−1H dipolar-driven 13C−13C recoupling without 13C rf irradiation in nuclear magnetic resonance of rotating solids. *J. Chem. Phys.* **2003**, *118*, 2325−2341.
(34) Fung, B. M.; Khitrin, A. K.; Ermolaev, K. An improved broadband decoupling sequence for liquid crystals and solids. *J. Magn. Reson.* **2000**, *142*, 97−101.
(35) Johnson, B. A. Using NMRView to visualize and analyze the NMR spectra of macromolecules. *Methods Mol. Biol.* **2004**, *278*, 313−352.
(36) Wang, Y.; Jardetzky, O. Probability-based protein secondary structure identification using combined NMR chemical-shift data. *Protein Sci.* **2002**, *11*, 852−861.
(37) Cavalli, A.; Salvatella, X.; Dobson, C. M.; Vendruscolo, M. Protein structure determination from NMR chemical shifts. *Proc. Natl. Acad. Sci. U. S. A.* **2007**, *104*, 9615−9620.
(38) Dasari, A. K. R.; Hung, I.; Michael, B.; Gan, Z.; Kelly, J. W.; Connors, L. H.; Griffin, R. G.; Lim, K. H. Structural characterization of cardiac ex vivo transthyretin amyloid: Insight into the transthyretin misfolding pathway in vivo. *Biochemistry* **2020**, *59*, 1800−1803.
(39) Palmieri, L. d. C.; Lima, L. M. T.; Freire, J. B.; Bleicher, L.; Polikarpov, I.; Almeida, F. C.; Foguel, D. Novel Zn2 -binding sites in human transthyretin: Implications for amyloidogenesis and retinol-binding protein recognition. *J. Biol. Chem.* **2010**, *285*, 31731−31741.
(40) Liu, K.; Cho, H. S.; Lashuel, H. A.; Kelly, J. W.; Wemmer, D. E. A glimpse of a possible amyloidogenic intermediate of transthyretin. *Nat. Struct. Biol.* **2000**, *7*, 754−757.
(41) Leach, B. I.; Zhang, X.; Kelly, J. W.; Dyson, H. J.; Wright, P. E. NMR measurements reveal the structural basis of transthyretin destabilization by pathogenic mutations. *Biochemistry (N. Y. )* **2018**, *57*, 4421−4430.
(42) Sun, X.; Dyson, H. J.; Wright, P. E. Fluorotryptophan incorporation modulates the structure and stability of transthyretin in a site-specific manner. *Biochemistry (N. Y. )* **2017**, *56*, 5570−5581.
(43) Lantz, C.; Rider, R. L.; Yun, S. D.; Laganowsky, A.; Russell, D. H. Water plays key roles in stabilities of wild type and mutant transthyretin complexes. *J. Am. Soc. Mass Spectrom.* **2024**, *35*, 1854−1864.
(44) Matwani, K.; Cornish, J.; DeBenedictis, E. A.; Heller, G. T. Micromolar fluoride contamination arising from glass NMR tubes and a simple solution for biomolecular applications. *J. Biomol. NMR.* **2024**, *78*, 161−167.
(45) Gibson, R. S.; Hess, S. Y.; Hotz, C.; Brown, K. H. Indicators of zinc status at the population level: A review of the evidence. *Br. J. Nutr.* **2008**, *99*, S14−S23.
(46) Kambe, T.; Tsuji, T.; Hashimoto, A.; Itsumura, N. The physiological, biochemical, and molecular roles of zinc transporters in zinc homeostasis and metabolism. *Physiol. Rev.* **2015**, *95*, 749−784.
(47) Sharma, M.; Khan, S.; Rahman, S.; Singh, L. R. The extracellular protein, transthyretin is an oxidative stress biomarker. *Front. Physiol.* **2019**, *10*, 5.
(48) Hurshman, A. R.; White, J. T.; Powers, E. T.; Kelly, J. W. Transthyretin aggregation under partially denaturing conditions is a downhill polymerization. *Biochemistry* **2004**, *43*, 7365−7381.
(49) Saelices, L.; Chung, K.; Lee, J. H.; Cohn, W.; Whitelegge, J. P.; Benson, M. D.; Eisenberg, D. S. Amyloid seeding of transthyretin by ex vivo cardiac fibrils and its inhibition. *Proc. Natl. Acad. Sci. U. S. A.* **2018**, *115*, E6741−E6750.

Downloaded from pubs.acs.org/bichaw/article-pdf/65/19/3017/6854085/acs.biochem.6c00448.pdf by FLORIDA STATE UNIV user on 02 November 2026


https://doi.org/10.1021/acs.biochem.6c00448
*Biochemistry* 2026, 65, 3017−3025